Journal of Membrane Science 671 (2023) 121407

Contents lists available at ScienceDirect

Journal of Membrane Science

journal homepage: www.elsevier.com/locate/memsci

Additive manufacturing of defect-healing polyamide membranes for fast and robust desalination

Dongwei Ma [a,b], Zhe Zhang [a,**], Sen Xiong [a], Jiemei Zhou [a], Yong Wang [a,*]

[a] State Key Laboratory of Materials-Oriented Chemical Engineering, College of Chemical Engineering, Nanjing Tech University, Nanjing, 211816, Jiangsu, PR China
[b] State Key Laboratory of Advanced Chemical Power Sources, Guizhou Meiling Power Sources Co. Ltd., Zunyi, 563003, Guizhou, PR China

ARTICLE INFO

Keywords:
Additive manufacturing
Spray-coating
Polyamide membrane
Interfacial polymerization
Defect-healing

ABSTRACT

Polyamide membranes that can exclude salts from water have found significant success in desalination applications. The polyamide thickness is difficult to control, as it is closely coupled with other properties including monomer chemistries and substrate structures. In this work, an additive manufacturing strategy using spray-coating to prepare large-area polyamide composite membranes with tunable thickness is explored. Using spray-coating, composite membranes comprising polyamide layers and carbon nanotube (CNT) layers on top of porous substrates are additively constructed. In the context of mediation by CNT layers, thickness control is decoupled from other properties. As a result, the polyamide thickness can be independently adjusted by changing monomer concentrations, and water permeance is found to be related to the thickness. A large-area membrane with a size of 30 × 30 cm^2 is successfully prepared under optimal conditions, and exhibits large water permeance of 34.1 L m^{-2} h^{-1} bar^{-1} and high Na_2SO_4 rejection rate of 95.6%. Importantly, the additive nature holds the ability to eliminate defects possibly existing through multiple spraying, affording defect-healing characteristic. This work allows envisioning a turning point that additive manufacturing is shifting the long-standing paradigm in the preparation of high-performance separation membranes.

1. Introduction

Nanofiltration is a prevalent membrane filtration technique that can separate salts from water efficiently, which is indispensable in the field of saline water desalination [1–3]. Thin-film composite (TFC) has served as a benchmark structure of nanofiltration membranes for more than three decades, which typically comprises a polyamide layer formed by interfacial polymerization, and an underlying porous substrate [4]. Interfacial polymerization occurs at an immiscible interface, in which piperazine (PIP) dissolving in water react with trimesoyl chloride (TMC) dissolving in *n*-hexane, forming a cross-linked polyamide nanofilm [5–7]. Considering the fast-reacting and irreversible nature of the aromatic acyl chloride and diamines [8], interfacial polymerization is governed by the reaction kinetics to a large extent. The reaction under conditions of kinetics control results in relatively uncontrollable growth of polyamide, the thickness of which is considered to be reversely proportional to its permeance. Furthermore, the variation of polyamide thickness is closely coupled with the properties of monomer chemistries and substrate structures [9]. Therefore, it remains a major challenge to tune the thickness of polyamide layers in a controllable and independent way.

To circumvent such vulnerability, some strategies have been proposed to decouple the thickness variation from other properties, enabling independent control [10–13]. Lee et al. reported a molecular layer-by-layer assembly [14]. Two types of reactive monomers were alternatively deposited on porous substrates to prepare polyamide membranes. The separation performance can be controlled exclusively by adjusting the deposition numbers, and the thickness control would not be limited to certain monomer chemistries. Livingston et al. employed a free aqueous-organic interface to access polyamide nanofilms with the thickness down to 8 nm [15]. Since no substrate was involved during interfacial polymerization, the thickness can be tuned independently by changing monomer concentrations. With the thickness decreasing, the water permeance was found to be increased proportionally. Nevertheless, both strategies require complex or additional processes to prepare composite membrane, which may become problematic in large-scale production. A promising alternative should have the ability to control the thickness independently but also be able to

* Corresponding author.
** Corresponding author.
E-mail addresses: zhangzhe@njtech.edu.cn (Z. Zhang), yongwang@njtech.edu.cn (Y. Wang).

https://doi.org/10.1016/j.memsci.2023.121407
Received 21 November 2022; Received in revised form 7 January 2023; Accepted 18 January 2023
Available online 19 January 2023

scale-up.

Additive manufacturing, also distinguished as 3D printing, is an emerging manufacturing technique that has found diverse applications in industry [16,17]. It holds an ability to construct, using various materials, geometrically complex architectures at different scale with high convenience and reproducibility [18]. Additive manufacturing has the benefit that allows each of material properties to be manipulated independently [19], while is capable of large-scale production. In this context, it provides a straightforward means by which the membrane thickness can be tuned in a controllable and independent way. Electro-spraying is a prime example of additive manufacturing that has been shown to be feasible for preparation of TFC polyamide membranes [20–22]. McCutcheon et al. proposed an electro-spraying strategy to prepare TFC polyamide membranes [23]. Applying a high electric field, monomer solutions in the form of small droplets were uniformly deposited on porous substrates in the presence of coulomb repulsion. By changing monomer concentrations and scanning numbers, the precise control of polyamide thickness was realized, and separation performances can be tuned accordingly.

Although scalable manufacturing using a roll-to-roll process for example was established, electro-spraying has inevitably required the use of an isolated chamber that is able to provide sustained and steady electric field. Our previous works have shown that spray-coating driven by compressed air is a convenient and flexible technique capable of preparing various separation membranes [24–28]. During spray-coating, liquid is atomized into uniform small droplets after leaving a nozzle. In this vein, polymers and nanomaterials can be evenly deposited onto arbitrary substrates. This process proceeds under ambient environment and no complex equipment is required, offering vast possibilities to be integrated with conventional manufacturing process. Therefore, the air-driven spraying can be regarded as an additive manufacturing method, not merely a simple spraying technique used to prepare membranes. Herein, we showed an additive manufacturing strategy to prepare large-area nanofiltration membranes with tunable thickness for fast and robust desalination (Scheme 1). TFC membranes were prepared by additive construction of carbon nanotube (CNT) layers and polyamide layers on top of macroporous polyether sulfone (PES) substrates. With the mediation of CNT layers, the thickness of polyamide layer can be independently tuned by changing monomer concentrations. The optimal TFC membrane showed a water permeance of 34.1 L m^{-2} h^{-1} bar^{-1} and a Na_2SO_4 rejection rate of 95.6%. Importantly, the additive nature endows this strategy with the capability of defect-healing that the defects can be eliminated by consecutively spraying.

2. Experimental sections

2.1. Materials

Multi-walled CNT (outer diameter: 4–6 nm, length: 10–20 μm, purity >95.0%) was provided by Nanjing XFNANO Materials Tech Co., Ltd. Pluronic F127 (M_w = 12.6 kDa) was obtained from Sigma-Aldrich. Piperazine (PIP, 99.0%), *n*-hexane (98.0%), sodium sulphate (Na_2SO_4, 99.5%), anhydrous magnesium sulphate ($MgSO_4$, 99.5%), magnesium chloride hexahydrate ($MgCl_2{\cdot}6H_2O$, 98.0%), sodium chloride (NaCl, 99.8%), *N,N*-dimethylformamide (DMF, 99.0%), and polyethylene glycol (PEG, M_w = 200, 400, 600, 1000, and 2000 Da) were purchased from Aladdin. Trimesoyl chloride (TMC, 98.0%) was obtained from J&K Scientific Co. Ltd. PES substrate with a nominal pore size of 0.45 μm was provided by Haiyan Xindongfang Plastic Technology Co., Ltd. Deionized (DI) water was used in all experiments.

2.2. Deposition of CNT on substrates

To prepare the CNT dispersion, CNT powders were first dispersed in water at a concentration of 0.5 mg mL^{-1}, followed by a sonication treatment at 650 W for 60 min. After that, a certain amount of Pluronic F127 was added to stabilize the dispersed CNT, and further subjected to the sonication at 100 W for another 30 min. As-obtained CNT dispersion was centrifuged at 10,000 rpm for 5 min to remove any aggregates possibly existing, and the supernatant was carefully collected as the final CNT dispersion. The CNT dispersion was spray-coated on PES substrates using a spraying equipment (SEV-300EDN, Suzhou Second Automatic Equipment Co., Ltd.). The air blow pressure was 1 bar, and spraying distance was 62 mm. The plate was maintained at 25 °C for evaporating water from the deposited CNTs. Typically, PES substrates with a size of 30 × 30 cm^2 were tiled on the plate of equipment, followed by spray-coating CNT dispersion onto substrates with an amount of 10 μL cm^{-2}. After dried at 25 °C, the CNT-coated PES substrates were obtained.

2.3. Preparation of membranes

The composite membranes (termed as PA-CNT membrane) were prepared by spray-assisted interfacial polymerization on CNT-coated PES substrates as illustrated in Scheme 1. Spraying conditions were same as above. PIP aqueous solutions with the concentrations ranging from 0.05% to 0.5% (w/v), as well as TMC *n*-hexane solutions with the concentrations ranging from 0.2% to 0.4% (w/v), were first prepared. The detailed conditions were listed in Table S1. CNT-coated PES substrates were soaked in PIP solutions for 30 s, and excess PIP solutions were subsequently removed by a rubber roller. The PIP solution-impregnated substrates were tiled on the spraying equipment,

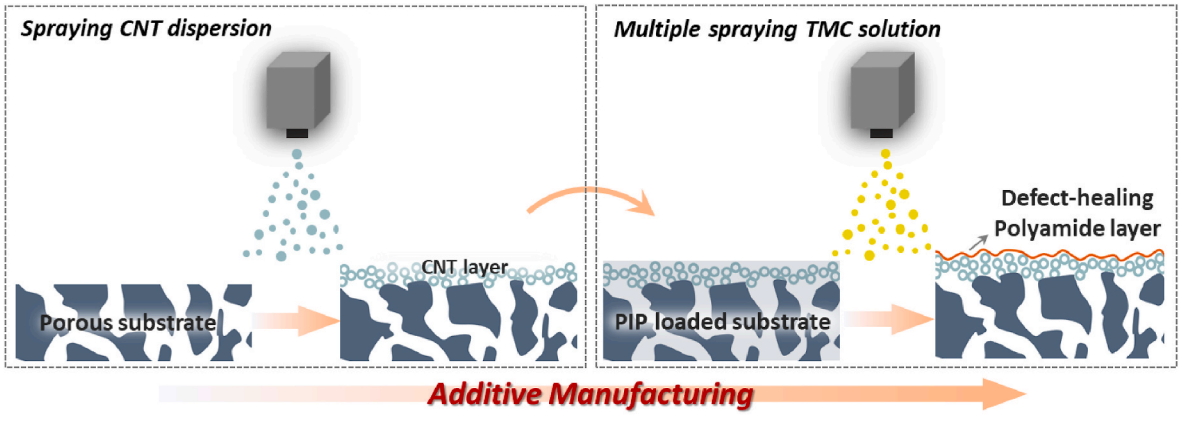

Scheme 1. Schematic diagram of the additive manufacturing of polyamide membranes.

followed by spray-coating TMC *n*-hexane solutions with designated concentrations. After interfacial polymerization, the membranes were cured in an oven at 70 °C for 10 min. The resultant membranes were stored in water for further use. In addition, control membranes (termed as PA membrane) were prepared using bare PES substrate, and the procedure was the same as above.

2.4. Characterizations

Microscopy observation of the membrane surfaces and cross sections was performed on a field-emission scanning electron microscope (SEM, Hitachi S4800) operating at a voltage of 5 kV and a probe current of 10 mA. All samples were sputter-coated with a layer of platinum to avoid discharging effect, prior to observation. Atomic force microscopy (AFM, XE-100, Park Systems) operating under a noncontact mode with a scanning speed of 0.5 Hz was used to measure the thickness of membranes. Membrane samples were obtained by etching away the PES substrates using DMF, and subsequently transferred onto silicon wafers to expose their thickness profiles. The membrane surface charges were analyzed by an electrokinetic analyzer (SurPASS, Anton Paar) under a streaming potential method using 1 mmol L^{-1} potassium chloride as the background electrolyte solution. The pH values during the test were in a range of 3–10.

2.5. Nanofiltration performance tests

Nanofiltration performances of membranes were tested using a cross-flow apparatus, of which the active filtration area was 7.1 cm^2. Prior to testing, all membranes were pressurized at 5 bar for 20 min to reach steady permeation flux. The test was conducted at 4 bar, and the cross-flow rate was 30 L h^{-1}. The temperature of the liquid was controlled by a heat exchanger at 25 °C. The permeation flux (J_w, L m^{-2} h^{-1}) and water permeance (P_w, L m^{-2} h^{-1} bar^{-1}) were calculated as follows:

$$J_w = \Delta V / (A\ \Delta t) \quad (1)$$

$$P_w = J_w / \Delta p \quad (2)$$

where ΔV (L) is the volume of the filtrate collected over a duration of Δt (h), A is the active filtration area (m^2), and Δp is the applied pressure (bar).

For the rejection test, the salt concentration in the feed solutions was 1000 mg L^{-1}. The rejection rate (R, %) of inorganic salts was calculated based on the conductivity of the feed C_p and the filtrate C_f using an electrical conductivity meter (S230-K, Mettler-Toledo) as below:

$$R = (1 - C_p / C_f) \times 100\% \quad (3)$$

To obtain the molecular weight cut-off (MWCO) of the membrane, the retention test using PEG with different molecular weights (200, 400, 600, 1000, and 2000 Da) was conducted. The concentration of PEG in the feed and the filtrate were measured by gel permeation chromatography (Waters 1515).

3. Results and discussion

3.1. Membranes prepared by additive manufacturing

In this work, the CNT dispersion was spray-coated on the PES substrate beforehand. After the deposition, the macropores of the PES substrate are covered by a continuous CNT layer (Fig. 1a and b). The macropores underlying the CNT layers still can be clearly seem, because of the ultrathin nature of CNT layers (Fig. 1b). After implementing spray-assisted interfacial polymerization at an optimal condition (PIP, 0.075%; TMC, 0.3%), a continuous and defect-free polyamide layer was formed atop the CNT-coated PES substrate (Fig. 1c). Likewise, the ultrathin nature of polyamide layer makes the underlying macropores visible. The cross-sectional SEM image reveals a triple-layered membrane structure that comprises a PES substrate, a CNT interlayer and a ~25 nm-thick polyamide layer (Fig. 1d). After etching away the PES substrate by DMF, a free-standing film composed of the polyamide layer and the CNT layer can be obtained (Fig. 1e). This film can be easily transferred onto a steel wire lasso, without compromising its structural integrity, due to the rigid and robust CNT networks. Based on the AFM analysis, the thickness of this film is ~95 nm (Fig. S1a). Notably, based on the same etching protocol, the thickness of CNT layer is measured to be ~70 nm (Fig. S1b). Thus, by subtracting the thickness of CNT layer,

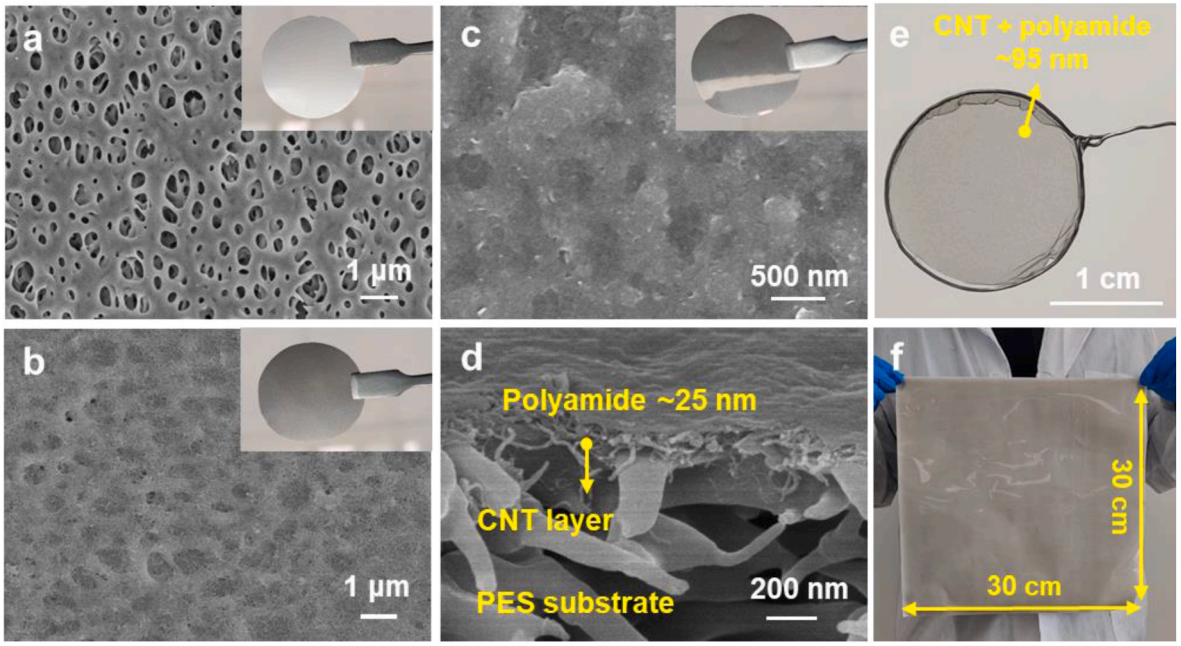

Fig. 1. Membrane preparation. SEM images of membrane surfaces (a–c) and cross sections (d). (a) PES substrate, (b) CNT-coated PES subsrate, (c) and (d) composite membranes. Insets show corresponding digital images. (e) Digital image of a free-standing membrane on a steel wire lasso. (f) Digital image of a large-area membrane with a size of 30 × 30 cm^2. The membranes were prepared at an optimal condition (PIP, 0.075%; TMC, 0.3%).

the thickness of polyamide layer is ~25 nm, which is in line with the observation from the cross-sectional SEM image. Importantly, large-area membranes, for example, 30 × 30 cm^2, was successfully prepared by this spray-assisted interfacial polymerization (Fig. 1f). During the preparation process, the organic solution was fully atomized and consequently sprayed onto the aqueous solution-impregnated membrane surface in an even and continuous way. Therefore, this spray-assisted interfacial polymerization can be considered as a flexible and scalable technique that is amenable to production of large-area membranes. Moreover, given the very thin thickness and the high specific surface area of the CNT layer, it can be firmly attached on the PES substrate, especially after drying treatment.

Fig. S2 displayed the influence of PIP concentrations on the membrane morphology. Increasing PIP concentrations from 0.05% to 0.5%, all membranes exhibit the relatively flat surface, except for the obvious defects appeared in the membrane prepared from the PIP concentration of 0.05%. In addition to the surface, the membrane thicknesses composed of the polyamide layer and the CNT layer enlarge from 82 nm to 185 nm, when PIP concentration increasing. The change of TMC concentrations on the membrane morphology were presented in Fig. S3. For lower PIP concentration (0.075%), the rise of TMC concentration leads to defect-free surface and slightly enlarged thickness. Similarly, in the case of higher PIP concentration (0.5%), the defects are eliminated and the thickness is enlarged, as TMC concentration rising. Considering that all membranes have almost same thickness of the CNT layer, the spray-assisted interfacial polymerization contributes to thin polyamide layers with the thickness down to ~12 nm. Importantly, this spray-assisted interfacial polymerization allows the thickness of polyamide layers to continuously adjust over a wide range of ~115 to ~12 nm.

3.2. Effects of CNT layers on membrane structures and performances

The CNT layers on PES substrates hold three critical characteristics: (i) mediation of interfacial polymerization to create minimal thickness; (ii) gutter effect for unobstructed water permeation; and (iii) providing adequate mechanical strength. As shown in Fig. 2a and d, the surface morphologies of PA and PA-CNT membrane are very similar, and both of them have relatively flat surfaces. The thickness of PA membrane is ~140 nm, while PA-CNT membrane has a thickness of ~48 nm (Fig. 2b and e). Note that such two membranes were prepared under same condition (PIP, 0.075%; TMC, 0.4%). The great divergence in thicknesses originates from the mediation of interfacial polymerization by CNT layers [29,30]. The PES substrate having large pores makes the interfacial polymerization very fast and relatively uncontrollable, thus resulting in large thicknesses [31]. Moreover, due to the strong wetting property of the PES substrate [32], the intrusion of the polyamide into macropores usually occurs [33], further increasing the thickness of the polyamide layer to some extent (Fig. 2c). In sharp contrast, a continuous layer of CNT network on top of the PES substrate would uptake and release of PIP aqueous solutions in a more controllable way [34], contributing to the formation of thinner polyamide layers [35]. Zeta potential test also confirms that controllable interfacial polymerization is likely to occur (Fig. S4). The reaction between PIP and TMC is very fast, thereby leaving a large number of unreacted acyl chlorides on the membrane surface. Those acyl chlorides would hydrolyze into carboxyl groups, which accounts for the high negative surface charge of PA membrane. Upon the mediation of interfacial polymerization by CNT layers, the reaction becomes more controllable through the controlled release of PIP, making the reaction between TMC and PIP more complete, and thus generating less unreacted acyl chlorides. As a result, the surface of PA-CNT membrane is in less negatively charged, evidencing the occurrence of controllable interfacial polymerization. Additionally, the continuous CNT layer offers a robust barrier that relieves the intrusion of the polyamide into the substrate macropores (Fig. 2f). Overall, in terms of mediation effect, the CNT layers on top of PES substrates are able to create polyamide layers with less thicknesses.

It is expected that CNT layers are beneficial to water transport from polyamide layers to PES substrates by means of gutter effect [29,36,37]. For typical composite membranes that merely comprise a polyamide layer and a porous substrate, water molecules need to transport through polyamide layers to the pore openings of substrates, assuming that polymeric backbone of substrates is impermeable. Thus, water molecules would transport in both vertical and slanting directions. Considering that the concentration gradient is normal to membrane surface, the transport occurring in vertical direction is regarded as the shortest path, which is in accordance with the thickness of the polyamide layer, and consequently minimizes the hydraulic resistance. For the transport far away from the pore openings, water molecules inevitably follow a slanting direction inside the polyamide layers, leaving an actual transport path being greatly larger than the thickness of polyamide layers. In this case, the transport occurring in slanting direction causes much higher hydraulic resistance.

As shown in Fig. 3a, with water molecules transporting both vertically and slantingly through the polyamide layer of PA membrane, it is

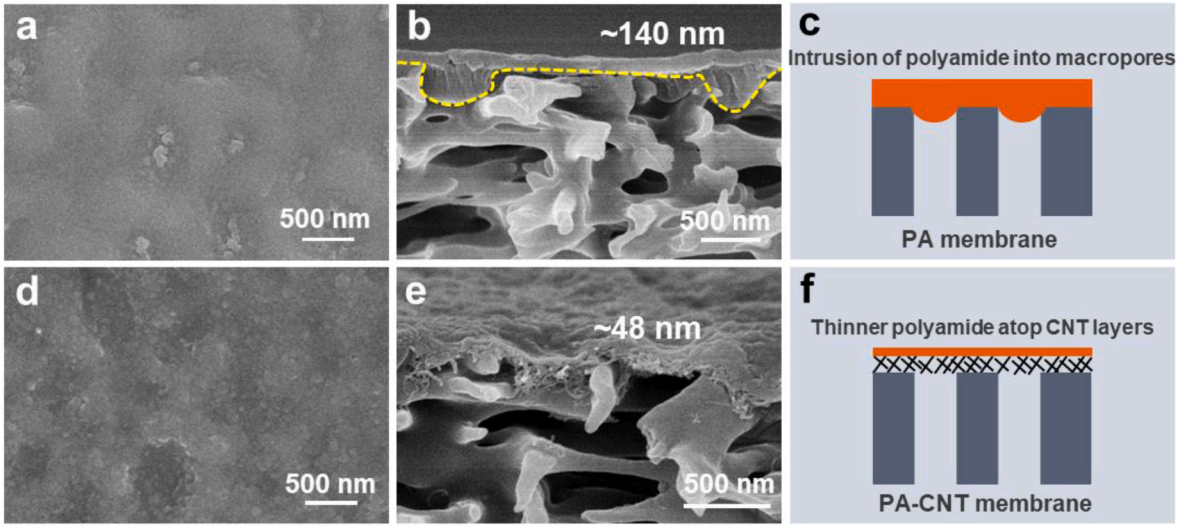

Fig. 2. Microstructures of different membranes. SEM images of (a) surface and (b) cross section of PA membrane. (c) Schematic illustration of PA membrane. SEM images of (d) surface and (e) cross section of PA-CNT membrane. (f) Schematic illustration of PA-CNT membrane. The membranes were prepared under same condition (PIP, 0.075%; TMC, 0.4%).

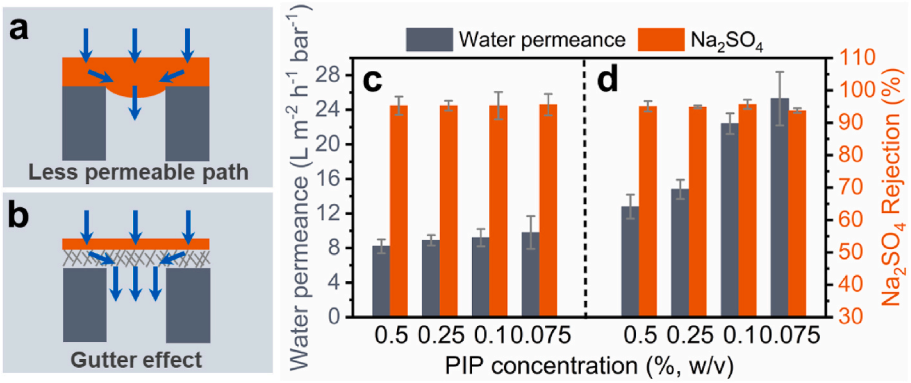

Fig. 3. Dissection the role of CNT layer. (a) Schematic depicting water transport through PA membrane. (b) Schematic depicting water transport through PA-CNT membrane. Effects of different PIP concentrations on the separation performance of PA (c) and PA-CNT membranes (d). The membranes were prepared under same TMC concentration of 0.4%.

necessary for water to take much longer transport path because of the large thickness. The intrusion of the polyamide occurring at the macropore would further increase thickness of the polyamide layer, thus extending the transport path. As a result, water transport inside PA membrane is subjected to high hydraulic resistance, leading to sluggish water permeation. As shown in Fig. 3b, the polyamide layer with a thin thickness has much lower hydraulic resistance, as the transport path is markedly shortened in vertical direction. Notably, the permeability of CNT network is much higher than that of the polyamide layer but close to that of the substrate. Water transport in the polyamide layer is more likely to occur along the vertical direction, instead of the transport in slanting direction that is observed in PA membrane. Water molecules still require to take longer transport path in CNT layer to reach the openings of the substrate. Nevertheless, the transport resistance in this case is significantly reduced, because of the high permeability of CNT network. Compared with thick polyamide layer of PA membrane, the CNT layer of PA-CNT membrane not only offer a shorter transport path, but also reduce the transport resistance. Therefore, the CNT layer can serve as a gutter layer that may offer a large number of shortcuts for fast water permeation.

To better understand the role of CNT layer, separation performances of PA and PA-CNT membranes were evaluated. The membranes were prepared from various PIP concentrations while TMC concentration was fixed at 0.4%. With PIP concentration decreasing from 0.5 to 0.075%, the water permeance enhanced while Na_2SO_4 rejection rate maintained almost unchanged for both membranes. In the case that the polyamide layer was directly formed on PES substrate (Fig. 3c), water permeance varied slightly in a range of ~8–10 L m^{-2} h^{-1} bar^{-1}. In contrast, water permeance increased sharply from ~12 to 25 L m^{-2} h^{-1} bar^{-1}, when the polyamide layer was formed on top of the CNT layer (Fig. 3d). In view of high hydraulic resistance stemming from large thickness and longer transport pass, the PA membrane was less permeable. Reducing the PIP concentration did not enhance the water permeance effectively, as the bare PES substrate was not able to mediate interfacial polymerization that creates thin polyamide layer for fast water permeation. Mediated by the CNT layer, a very thin layer of polyamide was formed, which exhibited less hydraulic resistance for water permeation. The CNT layer also served as a gutter layer, allowing water molecules easily to pass through, due to the high permeability of the CNT network. Thus, the water permeance of PA-CNT membranes regardless of PIP concentration was higher than that of PA membrane. Furthermore, the mediation effect of the CNT layer has the ability to control the thickness of the polyamide layer by changing PIP concentration, contributing to higher water permeance.

Typically, a polyamide layer having large thickness but low permeance is mechanically stable that can withstand high transmembrane pressure frequently required in nanofiltration process. However, a thin polyamide layer possessing large permeance seems to be mechanically problematic, and consequently is susceptible to high transmembrane pressure. To validate the influence of transmembrane pressure on separation performances, we prepared membranes with different structures. For the membrane with thick polyamide layer, with the pressure rising from 2 to 8 bar, the permeation flux was gradually enhanced, and Na_2SO_4 rejection rate slightly increased (Fig. 4a). Notably, the increase of the permeation flux was proportional to that of the pressure, indicating that the thick polyamide layer well maintained its structural integrity covering a wide range of pressures. Likewise, the polyamide layer having thin thickness exhibited a proportionally increased permeation flux and almost unchanged Na_2SO_4 rejection rate, when the pressure rising from 2 to 6 bar (Fig. 4b). However, the flux and Na_2SO_4 rejection rate were found to be compromised at a higher pressure of 8 bar. The thin polyamide layer directly formed on macroporous substrate may undergo significantly large stress at a higher transmembrane pressure, resulting in tearing or cracking that would deeply compromise separation performances [38]. In the context of a thin polyamide layer formed on the CNT layer, the permeation flux varied proportionally to the pressure change (Fig. 4c). The high pressure did not undermine the structural integrity as verified by the unchanged Na_2SO_4 rejection rate. The inherently strong π–π interaction of the CNT makes its layer mechanically robust [38–40]. Therefore, the CNT layer not only reinforces the structural integrity of thin polyamide layer, but also can scatter the stress and terminate the propagation of tearing or cracking possibly occurring.

3.3. Separation performance of membranes

To reveal the structure-property relationship, the separation performance of the PA-CNT membranes prepared under various PIP and TMC concentrations was evaluated (Fig. 5, Tables S2 and 3). With TMC concentration being fixed at 0.4%, water permeance of membranes was increasingly enhanced by lowering PIP concentration from 0.5 to 0.075% (Fig. 5a). Na_2SO_4 rejection rate did not vary when PIP concentration changing. This tendency was well related to the reduction of thickness of polyamide layers (Fig. S2), the membrane of which possessed almost same a PES substrate and a CNT layer. Under the lowest PIP concentration, that is, 0.05%, the membrane could not reject Na_2SO_4 effectively, because of the defect apparently existing on membrane surface (Fig. S2). To illustrate the separation performance influenced by various TMC concentrations, a high PIP concentration of 0.5% was first investigated. As shown in Fig. 5b, water permeance was markedly enhanced as TMC concentration dropped from 0.4 to 0.1%. Specifically, Na_2SO_4 rejection rate begun to decline slightly in the first conentration drop, while much pronounced decline of the rejection rate occurred in the next conentration drop. It seems that TMC being in lower

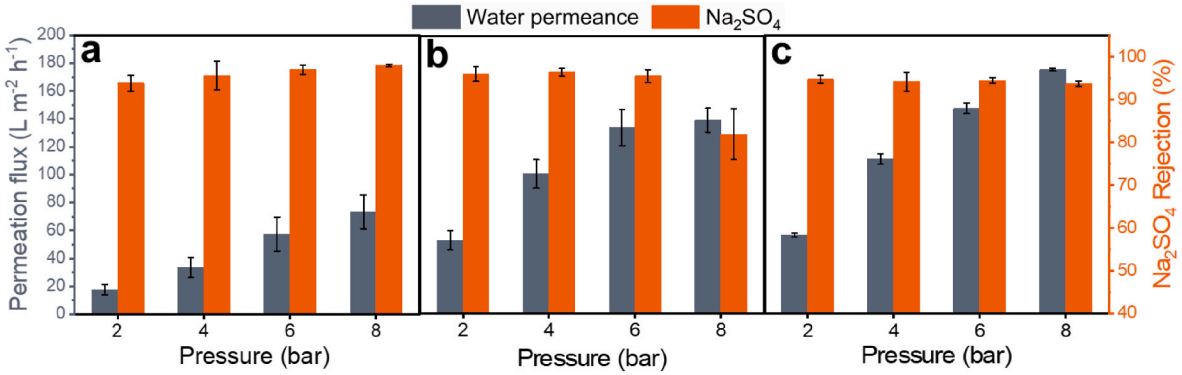

Fig. 4. Effects of pressure on the separation performance of different membranes. (a) Thick PA membrane (Condition: PIP, 0.075%; TMC, 0.4%). (b) Thin PA membrane (Condition: PIP, 0.075%; TMC, 0.1%). (c) PA-CNT membrane (Condition: PIP, 0.075%; TMC, 0.4%).

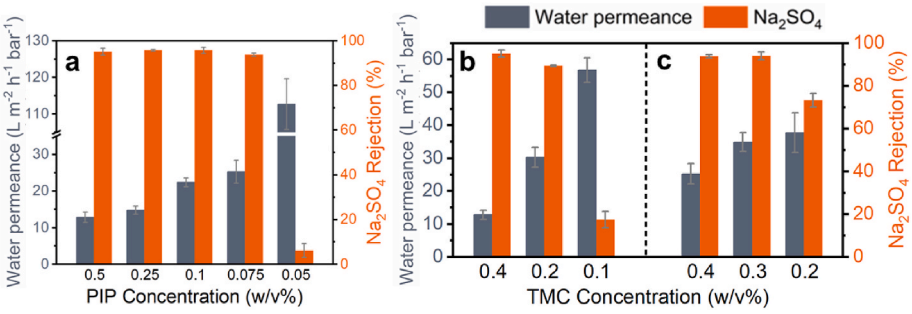

Fig. 5. Separation performance of PA-CNT membranes prepared from various PIP and TMC concentrations. (a) Effects of PIP concentration on water permeance and Na_2SO_4 rejection rate. TMC concentation was fixed at 0.4%. (b) and (c) Effects of TMC concentration on water permeance and Na_2SO_4 rejection rate. PIP concentation was fixed at 0.5% and 0.075% for (b) and (c), respectively.

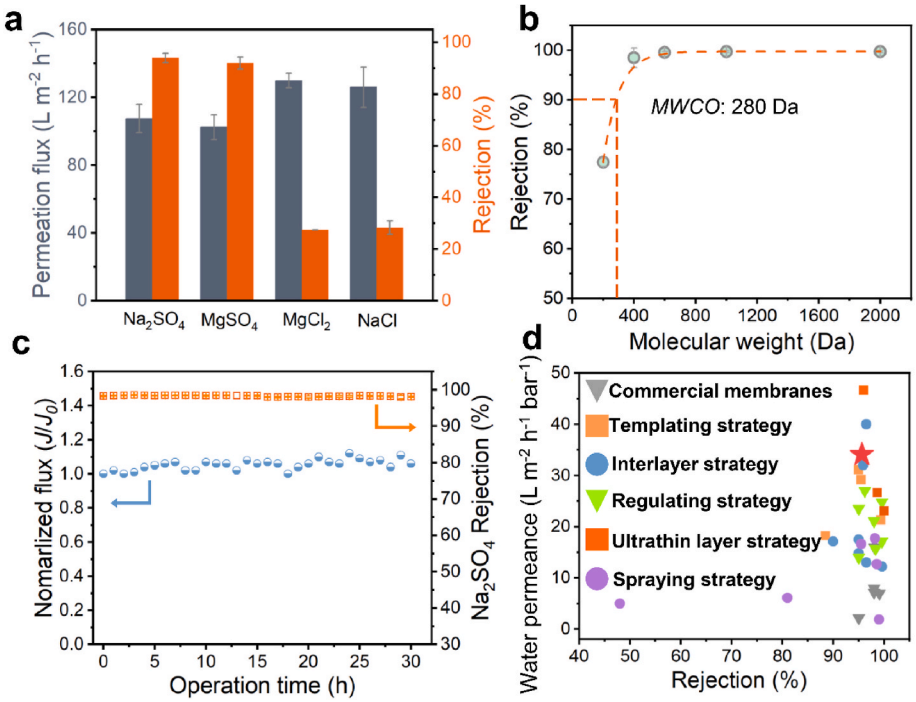

Fig. 6. Separation performance of PA-CNT membrane. (a) Permeation flux and rejection rate toward various inorganic salt solutions. (b) Characteristic curve of PEG retention. (c) Nanofiltration performance stability over a relatively long period of 30 h. (d) Nanofiltration performance of the membrane benchmarking against other state-of-the-art membranes and commercial membranes. The membranes were prepared at an optimal condition (PIP, 0.075%; TMC, 0.3%).

concentration would not be able to react thoroughly with PIP having higher concentration to form a defect-free polyamide layer. PIP molecules would diffuse from aqueous solution to the immiscible interface closer to the organic solution for the reaction with TMC. Thus, it is necessary for TMC to maintain a properly high concentration. Otherwise, rapid TMC consumption by excess PIP molecules would make the polyamide layer less cross-linked, leaving a large number of defects. In the case of lower PIP concentration of 0.075%, water permeance was progressively enhanced as TMC concentration dropped from 0.4 to 0.2% (Fig. 5c). Na_2SO_4 rejection rate was only compromised in a relatively low TMC concentration. The optimal separation performance can be obtained under a lower PIP concentration of 0.075%, and a higher TMC concentration of 0.3%. The water permeance was 34.1 L m^{-2} h^{-1} bar^{-1} and Na_2SO_4 rejection rate was 95.6%. The variation of separation performance under different TMC concentrations was also well related to the thickness change of polyamide layer (Fig. 3), as indicated previously. In addition, the separation performance of the large-area membrane with a size of 30 × 30 cm^2, which was mentioned above, was also tested (Table S4). The water permeance and Na_2SO_4 rejection rate were the same as that of the optimal membrane.

Fig. 6a displayed the permeation flux and rejection rate of the optimal membrane toward various inorganic salt solutions. The rejection characteristic of the membrane followed an order of Na_2SO_4, $MgSO_4$, $MgCl_2$, and NaCl. The separation performance of nanofiltration membranes is thought to be governed by a synergistic effect of steric hindrance and Donnan effect (electrostatic interaction). Divalent ions showed a higher rejection rate than that of the monovalent ion, which is ascribed to larger hydrated radius. Due to the negatively charged membrane surface, anions bearing more charges would undergo strong electrostatic repulsion than that of monovalent anion, resulting in higher rejection rate. In addition, other membranes prepared under various PIP and TMC concentrations (Tables S2 and S3) showed a similar rejection characteristic as referred above. The membrane possessed a relatively small MWCO of 280 Da (Fig. 6b). Once again this result evidenced that the defect-free membrane has the capability to desalination effectively. The permeation flux and Na_2SO_4 rejection rate maintained almost unchanged over a relatively long period of time (Fig. 6c), indicating that the membrane was defect-free and the significant compaction did not occur. The reinforcement derived from rigid and robust CNT network layer accounts for the excellent separation stability. To highlight the remarkable separation performance of our membrane, its water permeance and salt rejection were compared with other state-of-the-art membranes reported in literature (including several commercial membranes). Our membrane exhibited very high water permeance while maintaining a satisfactory salt rejection, outperforming most reported membranes prepared from various strategies (Fig. 6d and Table S5).

3.4. Defect-healing characteristic

The effective elimination of defects inevitably existing is prerequisite in the production of large-area membranes, which is thought to be a demanding challenge. In contrast to conventional interfacial polymerization that heavily relies on complex and time-consuming processes to eliminate defects, our strategy does not require extra processes but simply consecutively spraying TMC *n*-hexane solutions. As a demonstration (Fig. 7), we prepared a membrane with obvious defects using very low PIP concentration, which has been proved above. As result of the defects, this membrane exhibits very high water permeance but a negligible rejection rate to Na_2SO_4. When the spraying process repeating for only one time, the Na_2SO_4 rejection rate can radically rise from 6.2% to 98.6%, evidencing the complete elimination of defects. Since the CNT layer contains enough aqueous solutions, as-sprayed *n*-hexane solutions would contact with the aqueous solutions, triggering the reaction of TMC and PIP at local areas that had not been covered by polyamide layers. Thus, the polyamide continues to grow so as to form continuous and defect-free layers before the reaction is quenched by the self-limiting nature of interfacial polymerization [41]. As the spraying repeated for another time, the rejection rate maintains almost unchanged, while the water permeance continue to decline, due to the increased thickness. Given that the CNT layers have been wholly covered by polyamide layers after spraying repeated one-time, this barrier would segregate those two reaction phases. The increased thickness of polyamide layer mainly stems from the reaction between PIP and the unreacted acyl chlorides on the pre-formed polyamide. Therefore, our additive manufacturing strategy not only provides a nimble and cost-effective way to eliminate defects, but also endows polyamide membranes with defect-healing characteristic, which is of great significance for the large-scale production.

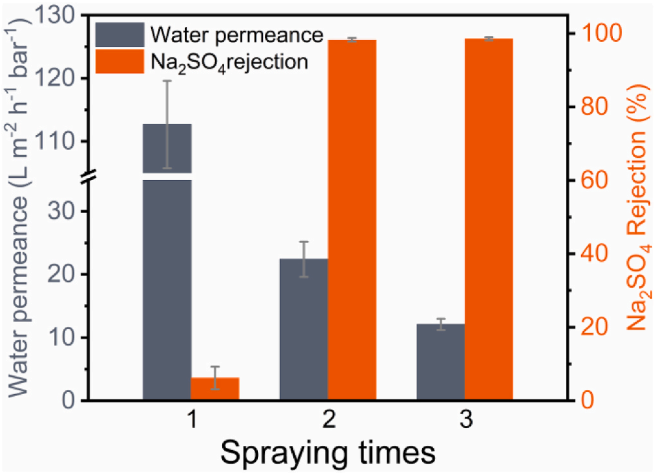

Fig. 7. Variation of spraying times of TMC *n*-hexane solutions on water permeance and Na_2SO_4 rejection.

4. Conclusions

In summary, an additive manufacturing strategy using spray-coating was proposed to prepare TFC polyamide membranes with tunable thickness. With the aid of spray-coating, TFC membranes featuring polyamide layers and CNT layers on top of PES substrates were constructed in an additive way. It is found that thickness control can be decoupled from other properties, as the mediation effect by CNT layers make interfacial polymerization more controllable. The polyamide thickness can be independently tuned by changing monomer concentrations, and water permeance was also related to the thickness. Using this approach, TFC membrane with a large size of 30 × 30 cm^2 was successfully constructed. The optimal membrane exhibited large water permeance of 34.1 L m^{-2} h^{-1} bar^{-1} and high Na_2SO_4 rejection rate of 95.6%. Importantly, additive nature endows membranes with defect-healing characteristic, which is beneficial to the large-scale production. Our work highlights the great promise of additive manufacturing, which may become a game changer in the preparation of high-performance separation membranes.

Author statement

Dongwei Ma: Conceptualization, Investigation, Data curation, Writing-original draft, Writing-review & editing, **Zhe Zhang:** Data curation, Writing-review & editing, Validation, **Sen Xiong:** Investigation, Methodology, **Jiemei Zhou:** Investigation, Methodology, Funding Acquisition, **Yong Wang**: Conceptualization, Writing-review & editing, Supervision, Funding Acquisition, All authors have approved to the final version of the manuscript.

Declaration of competing interest

The authors declare that they have no known competing financial interests or personal relationships that could have appeared to influence the work reported in this paper.

Data availability

Data will be made available on request.

Acknowledgments

Financial support from the Key Research and Development Program of the Jiangsu Provincial Department of Science and Technology of China (BE2022056-3) and the National Natural Science Foundation of China (21908095, 21825803).

Appendix A. Supplementary data

Supplementary data to this article can be found online at https://doi.org/10.1016/j.memsci.2023.121407.

References

[1] B. Park Ho, J. Kamcev, M. Robeson Lloyd, M. Elimelech, B.D. Freeman, Maximizing the right stuff: the trade-off between membrane permeability and selectivity, Science 356 (6343) (2017) eaab0530.
[2] J.R. Werber, C.O. Osuji, M. Elimelech, Materials for next-generation desalination and water purification membranes, Nat. Rev. Mater. 1 (5) (2016), 16018.
[3] M.A. Shannon, P.W. Bohn, M. Elimelech, J.G. Georgiadis, B.J. Mariñas, A. M. Mayes, Science and technology for water purification in the coming decades, Nature 452 (7185) (2008) 301–310.
[4] K. Zuo, K. Wang, R.M. DuChanois, Q. Fang, E.M. Deemer, X. Huang, R. Xin, I. A. Said, Z. He, Y. Feng, W. Shane Walker, J. Lou, M. Elimelech, X. Huang, Q. Li, Selective membranes in water and wastewater treatment: role of advanced materials, Mater. Today 50 (2021) 516–532.
[5] E.L. Wittbecker, P.W. Morgan, Interfacial polycondensation. I, J. Polym. Sci., Part A: Polym. Chem. 34 (4) (1996) 521–529.
[6] P.W. Morgan, S.L. Kwolek, Interfacial polycondensation. II. fundamentals of polymer formation at liquid interfaces, J. Polym. Sci., Part A: Polym. Chem. 34 (4) (1996) 531–559.
[7] F. Zhang, J.-B. Fan, S. Wang, Interfacial polymerization: from chemistry to functional materials, Angew. Chem. Int. Ed. 59 (49) (2020) 21840–21856.
[8] Z. Tan, S. Chen, X. Peng, L. Zhang, C. Gao, Polyamide membranes with nanoscale Turing structures for water purification, Science 360 (6388) (2018) 518–521.
[9] Y.J. Lim, K. Goh, G.S. Lai, Y. Zhao, J. Torres, R. Wang, Unraveling the role of support membrane chemistry and pore properties on the formation of thin-film composite polyamide membranes, J. Membr. Sci. 640 (2021), 119805.
[10] P. Sarkar, S. Modak, S. Ray, V. Adupa, K.A. Reddy, S. Karan, Fast water transport through sub-5 nm polyamide nanofilms: the new upper-bound of the permeance–selectivity trade-off in nanofiltration, J. Mater. Chem. 9 (36) (2021) 20714–20724.
[11] J. Zhu, J. Hou, R. Zhang, S. Yuan, J. Li, M. Tian, P. Wang, Y. Zhang, A. Volodin, B. Van der Bruggen, Rapid water transport through controllable, ultrathin polyamide nanofilms for high-performance nanofiltration, J. Mater. Chem. 6 (32) (2018) 15701–15709.
[12] C. Jiang, L. Zhang, P. Li, H. Sun, Y. Hou, Q.J. Niu, Ultrathin film composite membranes fabricated by novel in situ free interfacial polymerization for desalination, ACS Appl. Mater. Interfaces 12 (22) (2020) 25304–25315.
[13] C.-Y. Zhu, C. Liu, J. Yang, B.-B. Guo, H.-N. Li, Z.-K. Xu, Polyamide nanofilms with linearly-tunable thickness for high performance nanofiltration, J. Membr. Sci. 627 (2021), 119142.
[14] J.-E. Gu, S. Lee, C.M. Stafford, J.S. Lee, W. Choi, B.-Y. Kim, K.-Y. Baek, E.P. Chan, J. Y. Chung, J. Bang, J.-H. Lee, Molecular layer-by-layer assembled thin-film composite membranes for water desalination, Adv. Mater. 25 (34) (2013) 4778–4782.
[15] Z. Jiang, S. Karan, A.G. Livingston, Water transport through ultrathin polyamide nanofilms used for reverse osmosis, Adv. Mater. 30 (15) (2018), 1705973.
[16] A. Soo, S.M. Ali, H.K. Shon, 3D printing for membrane desalination: challenges and future prospects, Desalination 520 (2021), 115366.
[17] N. Yanar, P. Kallem, M. Son, H. Park, S. Kang, H. Choi, A New era of water treatment technologies: 3D printing for membranes, J. Ind. Eng. Chem. 91 (2020) 1–14.
[18] Z.-X. Low, Y.T. Chua, B.M. Ray, D. Mattia, I.S. Metcalfe, D.A. Patterson, Perspective on 3D printing of separation membranes and comparison to related unconventional fabrication techniques, J. Membr. Sci. 523 (2017) 596–613.
[19] X. Qian, M. Ostwal, A. Asatekin, G.M. Geise, Z.P. Smith, W.A. Phillip, R.P. Lively, J. R. McCutcheon, A critical review and commentary on recent progress of additive manufacturing and its impact on membrane technology, J. Membr. Sci. 645 (2022), 120041.
[20] S. Huang, J. Mansouri, P. Le-Clech, G. Leslie, C.Y. Tang, A.G. Fane, A comprehensive review of electrospray technique for membrane development: current status, challenges, and opportunities, J. Membr. Sci. 646 (2022), 120248.
[21] S. Yang, J. Wang, L. Fang, H. Lin, F. Liu, C.Y. Tang, Electrosprayed polyamide nanofiltration membrane with intercalated structure for controllable structure manipulation and enhanced separation performance, J. Membr. Sci. 602 (2020), 117971.
[22] X.-H. Ma, Z. Yang, Z.-K. Yao, H. Guo, Z.-L. Xu, C.Y. Tang, Interfacial polymerization with electrosprayed microdroplets: toward controllable and ultrathin polyamide membranes, Environ. Sci. Technol. Lett. 5 (2) (2018) 117–122.
[23] M.R. Chowdhury, J. Steffes, B.D. Huey, J.R. McCutcheon, 3D printed polyamide membranes for desalination, Science 361 (6403) (2018) 682–686.
[24] D. Ma, X. Ye, Z. Li, J. Zhou, D. Zhong, C. Zhang, S. Xiong, J. Xia, Y. Wang, A facile process to prepare fouling-resistant ultrafiltration membranes: spray coating of water-containing block copolymer solutions on macroporous substrates, Separ. Purif. Technol. 259 (2021), 118100.
[25] D. Ma, H. Li, Z. Meng, C. Zhang, J. Zhou, J. Xia, Y. Wang, Absolute and fast removal of viruses and bacteria from water by spraying-assembled carbon-nanotube membranes, Environ. Sci. Technol. 55 (22) (2021) 15206–15214.
[26] D. Ma, J. Zhou, Z. Wang, Y. Wang, Block copolymer ultrafiltration membranes by spray coating coupled with selective swelling, J. Membr. Sci. 598 (2020), 117656.
[27] D. Ma, X. Ye, X. Shi, J. Zhou, Y. Wang, Solvent-free process to high-flux ultrafiltration membranes: spray coating of water-dispersed carbon nanotubes, ACS ES&T Water 2 (5) (2022) 895–903.
[28] D. Ma, Z. Wang, T. Liu, Y. Hu, Y. Wang, Spray coating of polysulfone/poly(ethylene glycol) block polymer on macroporous substrates followed by selective swelling for composite ultrafiltration membranes, Chin. J. Chem. Eng. 29 (2021) 85–91.
[29] Z. Yang, P.-F. Sun, X. Li, B. Gan, L. Wang, X. Song, H.-D. Park, C.Y. Tang, A critical review on thin-film nanocomposite membranes with interlayered structure: mechanisms, recent developments, and environmental applications, Environ. Sci. Technol. 54 (24) (2020) 15563–15583.
[30] Z. Yang, F. Wang, H. Guo, L.E. Peng, X.-H. Ma, X.-X. Song, Z. Wang, C.Y. Tang, Mechanistic insights into the role of polydopamine interlayer toward improved separation performance of polyamide nanofiltration membranes, Environ. Sci. Technol. 54 (18) (2020) 11611–11621.
[31] L.E. Peng, Z. Yao, Z. Yang, H. Guo, C.Y. Tang, Dissecting the role of substrate on the morphology and separation properties of thin film composite polyamide membranes: seeing is believing, Environ. Sci. Technol. 54 (11) (2020) 6978–6986.
[32] M. Fathizadeh, A. Aroujalian, A. Raisi, Effect of lag time in interfacial polymerization on polyamide composite membrane with different hydrophilic sub layers, Desalination 284 (2012) 32–41.
[33] X. Ji, G. Li, G. Chen, Y. Qian, H. Jin, Z. Yao, L. Zhang, Aminated substrate based thin film composite nanofiltration membrane with high separation performance by chemically inhibiting the intrusion of polyamide, Desalination 532 (2022), 115724.
[34] Z. Yang, Z.-W. Zhou, H. Guo, Z. Yao, X.-H. Ma, X. Song, S.-P. Feng, C.Y. Tang, Tannic acid/Fe^{3+} nanoscaffold for interfacial polymerization: toward enhanced nanofiltration performance, Environ. Sci. Technol. 52 (16) (2018) 9341–9349.
[35] Z. Zhang, X. Shi, R. Wang, A. Xiao, Y. Wang, Ultra-permeable polyamide membranes harvested by covalent organic framework nanofiber scaffolds: a two-in-one strategy, Chem. Sci. 10 (39) (2019) 9077–9083.
[36] F. Wang, Z. Yang, C.Y. Tang, Modeling water transport in interlayered thin-film nanocomposite membranes: gutter effect vs funnel effect, ACS ES&T Engg 2 (11) (2022) 2023–2033, 2022.
[37] L. Long, C. Wu, Z. Yang, C.Y. Tang, Carbon nanotube interlayer enhances water permeance and antifouling performance of nanofiltration membranes: mechanisms and experimental evidence, Environ. Sci. Technol. 56 (4) (2022) 2656–2664.
[38] Y. Yang, X. Yang, L. Liang, Y. Gao, H. Cheng, X. Li, M. Zou, R. Ma, Q. Yuan, X. Duan, Large-area graphene-nanomesh/carbon-nanotube hybrid membranes for ionic and molecular nanofiltration, Science 364 (6445) (2019) 1057–1062.
[39] M.-B. Wu, Y. Lv, H.-C. Yang, L.-F. Liu, X. Zhang, Z.-K. Xu, Thin film composite membranes combining carbon nanotube intermediate layer and microfiltration support for high nanofiltration performances, J. Membr. Sci. 515 (2016) 238–244.
[40] Z. Zhou, Y. Hu, C. Boo, Z. Liu, J. Li, L. Deng, X. An, High-performance thin-film composite membrane with an ultrathin spray-coated carbon nanotube interlayer, Environ. Sci. Technol. Lett. 5 (5) (2018) 243–248.
[41] S. Zhou, L. Long, Z. Yang, S.L. So, B. Gan, H. Guo, S.-P. Feng, C.Y. Tang, Unveiling the growth of polyamide nanofilms at water/organic free interfaces: toward enhanced water/salt selectivity, Environ. Sci. Technol. 56 (14) (2022) 10279–10288.